Available online at www.sciencedirect.com
SCIENCE DIRECT®
PERGAMON
International Journal of Heat and Mass Transfer 46 (2003) 4681–4693
International Journal of HEAT and MASS TRANSFER
www.elsevier.com/locate/ijhmt

A new stochastic approach to transient heat conduction modeling with uncertainty

Dongbin Xiu, George Em Karniadakis *

Center for Fluid Mechanics, Division of Applied Mathematics, Brown University, 182 George Street, Box F, Providence, RI 02912 USA

Received 1 November 2002; received in revised form 12 May 2003

Abstract

We present a generalized polynomial chaos algorithm for the solution of transient heat conduction subject to uncertain inputs, i.e. random heat conductivity and capacity. The stochastic input and solution are represented spectrally by the orthogonal polynomial functionals from the Askey scheme, as a generalization of the original polynomial chaos idea of Wiener [Am. J. Math. 60 (1938) 897]. A Galerkin projection in random space is applied to derive the equations in the weak form. The resulting set of deterministic equations is subsequently discretized by the spectral/*hp* element method in physical space and integrated in time. Numerical examples are given and the convergence of the chaos expansion is demonstrated for a model problem.

Keywords: Uncertainty; Stochastic modeling; Polynomial chaos; Transient heat conduction; Random medium

1. Introduction

Heat transfer analysis relies heavily on obtaining accurate physical properties of the medium. In many situations, experimental data for physical properties are available, but there exist cases where obtaining them is a difficult task and appropriate models have to be used. For example, obtaining physical properties from measurements for gas mixtures at high temperatures can be difficult. Both measurement-based and model-based physical properties are subject to errors (random, systematic and modeling errors) and determining the effect of these errors becomes essential in heat transfer design. In some cases, especially in complex systems, the effect of these uncertainties can be significant. For instance, it has been shown that the uncertainty in heat conductivity has substantial influence on the temperature prediction of biological bodies [24]. The resulting temperature uncertainty is very important in treatment planning and in designing certain clinical apparatus where even a few degrees of temperature fluctuation may cause serious problem [7].

It is a common practice in engineering to use mean values for design variables or parameters and then use safety factors to specify the final design. Safety factors tend to overspecify the equipment, increasing both manufacturing and operating costs. Thus, there has been recently a growing interest in probabilistic modeling for uncertainty quantification and sensitivity analysis. Such probabilistic modeling can be implemented by using either a statistical approach or a non-statistical approach. The statistical approach, e.g. Monte Carlo simulation (MCS), employs repetitive tests over a sufficiently large body of sampling. On the other hand, the non-statistical approach is based upon an analytical treatment of the uncertainty. In many cases, it has advantages over the statistical approach in terms of computer time and in ease of interpretation. Thus, recent research effort has been focusing on developing efficient non-statistical methods for uncertainty quantification.

Several non-statistical methods have been developed with different treatment of stochastic fields. The perturbation method is based on the expansion of random quantities around their mean values, and is widely used in practice. The solution is often expressed in terms of

* Corresponding author. Fax: +1-401-863-3369.
E-mail address: gk@cfm.brown.edu (G.E. Karniadakis).

0017-9310/$ - see front matter © 2003 Elsevier Ltd. All rights reserved.
doi:10.1016/S0017-9310(03)00299-0

their first- and second-moment, resulting in the so-called 'second moment analysis' [22,25,27,26,31]. Another approach is based on the manipulation of the stochastic operator. Methods along this line of approach include the weighted integral method [9,10] and Neumann expansion method [30,39]. In [8], a formulation based on finite element method was proposed to 'discretize' directly the random field.

A non-statistical approach, called polynomial chaos, is based on the homogeneous chaos theory of Wiener [33]. This method was first applied by Ghanem and Spanos to various problems in mechanics [12–16]. It involves a spectral expansion of random variables based on the *Hermite* orthogonal polynomials in terms of *Gaussian* random variables. A broader framework, called the 'generalized polynomial chaos' or the 'Wiener–Askey chaos', was proposed in [36]. This method employs more orthogonal polynomials from the Askey scheme [1] as the expansion basis to represent general *non-Gaussian* processes more efficiently. It includes the classical Hermite polynomial chaos as a subset and has been applied to various problems [37,35,38].

The objective of this paper is to model transient heat conduction with uncertain inputs by the generalized polynomial chaos expansion. In particular, we focus on media with random heat conductivity and capacity. The corresponding steady-state problem has been studied both theoretically and numerically [2–5,8,17]. A number of papers have addressed the unsteady problems, using perturbation methods [11,18–20] and the classical Hermite polynomial chaos in one physical dimension [13].

In this paper, we solve the two-dimensional unsteady heat transfer problem by generalized polynomial chaos expansion, where the uncertainties can be introduced through heat conductivity, heat capacity, source terms, boundary/initial conditions or some combinations. In the next section, we review the concept of the generalized polynomial chaos, and in Section 3 the Karhunen–Loeve expansion for representation of the stochastic inputs. In Section 4, we apply the expansion to the unsteady heat conduction equation. Numerical results are presented in Section 5, and we conclude the paper with a brief discussion.

2. Generalized polynomial chaos (Wiener–Askey chaos)

The generalized polynomial chaos expansion is a representation of a function $f \in L_2(\Omega)$ where Ω is the properly defined probability space. It employs the hypergeometric orthogonal polynomials from the Askey scheme in the random space as the trial basis to expand stochastic processes. The Askey scheme classifies the hypergeometric orthogonal polynomials and indicates the limit relations between them. For a detailed account of definitions and properties of hypergeometric polynomials, see [1]; for the limit relations of the Askey scheme, see [23] and [29].

The original polynomial chaos [33,34] employs the Hermite polynomials in the random space as the trial basis. Cameron and Martin [6] proved that such expansion converges to any second-order processes in the L_2 sense. The generalized polynomial chaos, or the Wiener–Askey chaos, includes more types of orthogonal polynomials from the Askey scheme, and the classical Hermite polynomial chaos is a subset.

The representation of a general second-order random process $X(\omega)$ by generalized polynomial chaos can be expressed as

$$\begin{aligned} X(\omega) = {} & c_0 \Psi_0 + \sum_{i_1=1}^{\infty} c_{i_1} \Psi_1\left(\xi_{i_1}(\theta)\right) \\ & + \sum_{i_1=1}^{\infty} \sum_{i_2=1}^{i_1} c_{i_1 i_2} \Psi_2\left(\xi_{i_1}(\theta), \xi_{i_2}(\theta)\right) \\ & + \sum_{i_1=1}^{\infty} \sum_{i_2=1}^{i_1} \sum_{i_3=1}^{i_2} c_{i_1 i_2 i_3} \Psi_3\left(\xi_{i_1}(\theta), \xi_{i_2}(\theta), \xi_{i_3}(\theta)\right) \\ & + \cdots, \end{aligned} \tag{1}$$

where $\Psi_n(\xi_{i_1}, \ldots, \xi_{i_n})$ denotes the *generalized polynomial chaos* of order n in terms of the multi-dimensional random variables $\boldsymbol{\xi} = (\xi_1, \ldots, \xi_n, \ldots)$. Note that this is an infinite summation in the infinite dimensional space of $\boldsymbol{\xi}$. The expansion bases $\{\Psi_n\}$ are multi-dimensional hypergeometric polynomials defined as tensor-products of the corresponding one-dimensional polynomials bases $\{\phi_k\}_{k=0}^{\infty}$, which form an orthogonal basis in $L_2(\mathbb{R})$. The corresponding type of polynomials $\{\Psi\}$ and their associated random variables $\boldsymbol{\xi}$ are listed in Table 1.

Table 1
Correspondence of the orthogonal polynomials and random variables for different Wiener–Askey chaos ($N \geqslant 0$ is a finite integer)

	Random variables $\boldsymbol{\xi}$	Orthogonal polynomials $\{\Phi_n\}$	Support
Continuous	Gaussian	Hermite	$(-\infty, \infty)$
	Gamma	Laguerre	$[0, \infty)$
	Beta	Jacobi	$[a, b]$
	Uniform	Legendre	$[a, b]$
Discrete	Poisson	Charlier	$\{0, 1, 2, \ldots\}$
	Binomial	Krawtchouk	$\{0, 1, \ldots, N\}$
	Negative binomial	Meixner	$\{0, 1, 2, \ldots\}$
	Hypergeometric	Hahn	$\{0, 1, \ldots, N\}$

For notational and computational convenience, Eq. (1) is often rewritten, according to some numbering scheme, in a form with only one index as

$$X(\omega) = \sum_{j=0}^{\infty} a_j \Phi_j(\xi(\omega)), \tag{2}$$

where there is a one-to-one correspondence between the coefficients and basis functions in (1) and (2). The family $\{\Phi_n\}$ is an orthogonal basis in $L_2(\Omega)$ with orthogonality relation

$$\langle \Phi_i \Phi_j \rangle = \langle \Phi_i^2 \rangle \delta_{ij}, \tag{3}$$

where δ_{ij} is the Kronecker delta and $\langle \cdot, \cdot \rangle$ denotes the ensemble average which is the inner product in the Hilbert space of the variables $\boldsymbol{\xi}$

$$\begin{aligned} \langle f(\boldsymbol{\xi}) g(\boldsymbol{\xi}) \rangle &= \int f(\boldsymbol{\xi}) g(\boldsymbol{\xi}) W(\boldsymbol{\xi}) \, \mathrm{d}\boldsymbol{\xi}, \quad \text{or} \\ \langle f(\boldsymbol{\xi}) g(\boldsymbol{\xi}) \rangle &= \sum_{\boldsymbol{\xi}} f(\boldsymbol{\xi}) g(\boldsymbol{\xi}) W(\boldsymbol{\xi}) \end{aligned} \tag{4}$$

in the discrete case. Here $W(\boldsymbol{\xi})$ is the weighting function corresponding to the Askey polynomials chaos basis $\{\Phi_i\}$.

In the Wiener–Askey chaos expansion, the type of the orthogonal polynomials $\{\Phi_n\}$ is chosen in such a way that their weighting function has the same form as the probability function of $\boldsymbol{\xi}$. As an example, we show the Wiener–Jacobi chaos in one dimension. The one-dimensional nth-order Jacobi polynomials are defined as

$$\begin{aligned} P_n^{(\alpha,\beta)}(\xi) = {} & \frac{(-1)^n}{2^n n!} (1-\xi)^{-\alpha} (1+\xi)^{-\beta} \\ & \times \frac{\mathrm{d}^n}{\mathrm{d}x^n} \left[(1-\xi)^{n+\alpha} (1+\xi)^{n+\beta} \right], \quad -1 < \xi < 1, \end{aligned} \tag{5}$$

where parameter α, $\beta > -1$ are real numbers. The weight function in the orthogonality relation (4) is

$$W(\xi; \alpha, \beta) = \frac{(1-\xi)^{\alpha} (1+\xi)^{\beta}}{2^{\alpha+\beta+1} B(\alpha+1, \beta+1)}, \quad -1 < \xi < 1, \tag{6}$$

where $B(p,q) = \Gamma(p)\Gamma(q)/\Gamma(p+q)$ is the beta function. It can be seen that this weighting function is in the same form as the probability density function (PDF) of a β random variable defined in $(-1, 1)$. The first few members of the one-dimensional Wiener–Jacobi chaos are

$$\Phi_0 = 1, \quad \Phi_1 = \frac{\alpha+\beta+2}{2} \xi + \frac{\alpha-\beta}{2}, \ldots \tag{7}$$

When $\alpha = \beta = 0$, the Wiener–Jacobi chaos reduces to Wiener–Legendre chaos with weighting function $W(\xi) = 1/2$, $-1 < \xi < 1$, which is the PDF of the uniform random variable $\xi \sim U(-1, 1)$. Within the framework of generalized polynomial chaos, one has more freedom to represent general non-Gaussian stochastic processes more efficiently. For more details about generalized polynomial chaos, see [35,36,37].

3. The Karhunen–Loeve decomposition

The Karhunen–Loeve (KL) expansion is another way of representing a random process [28]. It is based on the spectral expansion of the correlation function of the process. It is particularly useful for the generalized polynomial chaos expansion as it provides a means of reducing dimensionality in random space. Let us denote the process by $h(\mathbf{x}; \omega)$ and its correlation function by $R_{hh}(\mathbf{x}, \mathbf{y})$, where $\mathbf{x}$ and $\mathbf{y}$ are the spatial or temporal coordinates. The KL expansion then takes the following form:

$$h(\mathbf{x}; \omega) = \bar{h}(\mathbf{x}) + \sum_{i=1}^{\infty} \sqrt{\lambda_i} \phi_i(\mathbf{x}) \xi_i(\omega), \tag{8}$$

where $\bar{h}(\mathbf{x})$ denotes the mean of the random process, and $\xi_i(\omega)$ forms a set of uncorrelated random variables. Also, $\phi_i(\mathbf{x})$ and λ_i are the eigenfunctions and eigenvalues of the correlation function, respectively, i.e.,

$$\int R_{hh}(\mathbf{x}, \mathbf{y}) \phi_i(\mathbf{y}) \, \mathrm{d}\mathbf{y} = \lambda_i \phi_i(\mathbf{x}). \tag{9}$$

In practice, a finite-term expansion of (8) is employed, where the summation is truncated at finite number n. The number of terms n is determined by the decay of eigenvalues from (9) to ensure the truncation error is acceptably small. Subsequently, this results in an n-dimensional polynomial chaos expansion, with each term from (8) corresponding to the linear (first-order) terms in the chaos expansion. Among other possible decompositions of a random process, the KL expansion is optimal in the sense that the mean-square error of the finite-term representation is minimized. It provides an effective way to represent the input random processes with known correlation function.

4. Governing equations and solution procedure

The unsteady stochastic heat equation for a spatially varying medium, in the absence of convection, is

$$\begin{aligned} & c(x; \omega) \frac{\partial T}{\partial t} = \nabla \cdot [\mathbf{k}(x; \omega) \nabla T] + f(t, x; \omega), \\ & (x, \omega) \in D \times \Omega \end{aligned} \tag{10}$$

subjected to the following initial and boundary conditions

$$T(0, x; \omega) = T_0(x, \omega), \tag{11}$$

$$\begin{aligned} & T(t, x; \omega) = T_b, \ \ x \in \partial D_1, \quad -\mathbf{k} \frac{\partial T}{\partial n}(t, x; \omega) = q_b, \\ & x \in \partial D_2, \end{aligned} \tag{12}$$

where D is a bounded domain in $\mathbb{R}^d$ ($d = 1, 2, 3$) and Ω is a probability space. The temperature $T \equiv T(t, x; \omega)$ and heat source $f(t, x; \omega)$ are $\mathbb{R}$-valued functions on $[0, \infty] \times D \times \Omega$. The initial condition T_0 and the volumetric heat capacity of the medium c are $\mathbb{R}$-valued functions on $D \times \Omega$, and $\mathbf{k}(\mathbf{x}; \omega) = [k_{ij}(x, \omega)]$ is the conductivity tensor defined on $D^{d\times d} \times \Omega$. ∂D_1 and ∂D_2 denote the subsets of the boundary with fixed temperature and heat flux, respectively. We further assume that the medium is isotropic with $k_{ii}(x) = k(x)$, $\forall i \in [1, d]$ and $k_{ij} = 0$, $i \neq j$. The governing equation (10) can be rewritten as

$$c(x;\omega)\frac{\partial T}{\partial t} = \nabla \cdot [k(x;\omega)\nabla T] + f(t,x;\omega), \quad (x,\omega) \in D \times \Omega \tag{13}$$

with initial condition (11) and boundary condition (12). Note this assumption on $\mathbf{k}$ simplifies the demonstration of the algorithm, but does not limit its applicability.

By using the generalized chaos expansion, we expand the random processes in the system of (13), (11) and (12) in the following form:

$$\begin{aligned} k(x;\omega) &= \sum_{i=0}^{M} k_i(x)\Phi_i(\boldsymbol{\xi}), \\ T(t,x;\omega) &= \sum_{i=0}^{M} T_i(t,x)\Phi_i(\boldsymbol{\xi}), \\ f(t,x;\omega) &= \sum_{i=0}^{M} f_i(t,x)\Phi_i(\boldsymbol{\xi}). \end{aligned} \tag{14}$$

Note here we have replaced the infinite summation of $\boldsymbol{\xi}$ in infinite dimensions in Eq. (2) by a truncated finite-term summation of $\{\Phi\}$ in the finite dimensions of $\boldsymbol{\xi} = (\xi_1, \ldots, \xi_n)$. The dimensionality n of $\boldsymbol{\xi}$ is determined by the random inputs. The random parameter ω is absorbed into the polynomial basis $\Phi(\boldsymbol{\xi})$, thus the expansion coefficients k_i, T_i and f_i are deterministic. Similar expansions are applied to other quantities c, T_0, T_b and q_b. By substituting the expansion into governing equation (13), we obtain

$$\sum_{i=0}^{M} c_i(x)\Phi_i \sum_{j=0}^{M} \frac{\partial T_j}{\partial t}\Phi_j = \nabla \cdot \left[\sum_{i=0}^{M} k_i(x)\Phi_i \nabla\left(\sum_{j=0}^{M} T_j(t,x)\Phi_j\right)\right] + \sum_{i=0}^{M} f_i(t,x)\Phi_i. \tag{15}$$

A Galerkin projection of the above equation onto each polynomial basis $\{\Phi_i\}$ is then conducted in order to ensure that the error is orthogonal to the functional space spanned by the finite-dimensional basis $\{\Phi_i\}$. By projecting with Φ_k for each $k = \{0, \ldots, M\}$ and employing the orthogonality relation (3), we obtain for each $k = 0, \ldots, M$

$$\sum_{i=0}^{M}\sum_{j=0}^{M} c_i(x)\frac{\partial T_j}{\partial t}e_{ijk} = \sum_{i=0}^{M}\sum_{j=0}^{M} \nabla \cdot \left[k_i(x)\nabla T_j(t,x)\right]e_{ijk} + f_k(t,x)\langle\Phi_k^2\rangle, \tag{16}$$

where $e_{ijk} = \langle\Phi_i\Phi_j\Phi_k\rangle$. Together with $\langle\Phi_i^2\rangle$, the coefficients e_{ijk} can be evaluated analytically from the definition of Φ_i. By defining

$$b_{jk}(x) = \sum_{i=0}^{M} c_i(x)e_{ijk}, \quad s_{jk}(x) = \sum_{i=0}^{M} k_i(x)e_{ijk}$$

we can rewrite the above equation as

$$\sum_{j=0}^{M} b_{jk}(x)\frac{\partial T_j}{\partial t}(t,x) = \sum_{j=0}^{M} \nabla \cdot \left[s_{jk}(x)\nabla T_j(t,x)\right] + f_k(t,x)\langle\Phi_k^2\rangle \quad \forall k \in [0, M]. \tag{17}$$

Eq. (17) is a set of $(M + 1)$ coupled partial differential equations. The total number of equations $(M + 1)$ is determined by the dimensionality of the chaos expansion (n) and the highest order (p) of the polynomials $\{\Phi\}$, where

$$(M + 1) = (n + p)!/(n!p!). \tag{18}$$

The initial condition (11) and boundary condition (12) are expanded in the same form as (14). By matching the coefficients in the expansions, we obtain the initial conditions and boundary conditions for each expanded equation in (17) to complete the system.

By defining $\mathbf{B}(x) = [b_{ij}(x)]$, $\mathbf{S}(x) = [s_{ij}(x)]$ with the indices running through $[0, \ldots, M]$ and solution vector $\mathbf{T}(t,x) = [T_0(t,x), T_1(t,x), \ldots, T_M(t,x)]^t$, Eq. (17) can be written more concisely as

$$\mathbf{B}(x)\frac{\partial \mathbf{T}}{\partial t}(t,x) = \nabla \cdot [\mathbf{S}(x)\nabla \mathbf{T}(t,x)] + \mathbf{F}(t,x), \tag{19}$$

where $\mathbf{F}(x) = [f_0\langle\Phi_0^2\rangle, \ldots, f_M\langle\Phi_M^2\rangle]^t$. Here we have used the symmetry of matrices $\mathbf{B}(x)$ and $\mathbf{S}(x)$, i.e. $\mathbf{B}(x) = \mathbf{B}^t(x)$ and $\mathbf{S}(x) = \mathbf{S}^t(x)$. It can be seen that each expansion mode of the solution $T_i(t,x)$, $i \in [0, \ldots, M]$ in (19) is coupled on the left-hand side and the right-hand side. In order to solve the equation efficiently, we invert the matrix $\mathbf{B}(x)$ such that $\mathbf{D}(x) \equiv [d_{ij}(x)] = \mathbf{B}^{-1}(x)$ and rewrite (19) as

$$\frac{\partial \mathbf{T}}{\partial t}(t,x) = \mathbf{D}(x)\nabla \cdot [\mathbf{S}(x)\nabla \mathbf{T}(t,x)] + \mathbf{D}(x)\mathbf{F}(t,x) \tag{20}$$

or, in index form, $\forall k \in [0, \ldots, M]$

$$\frac{\partial T_k}{\partial t}(t,x) = \sum_{i=0}^{M}\sum_{j=0}^{M} d_{kj}(x)\nabla \cdot \left[S_{ji}(x)\nabla T_i(t,x)\right] + \sum_{i=0}^{M} d_{ki}(x)f_i(t,x)\langle\Phi_i^2\rangle. \tag{21}$$

The left-hand side is then decoupled and the equations can be integrated successively in time. To avoid the se-

Table 2
Coefficients in the mixed explicit–implicit integration (23) (see [21], chapter 8)

Coefficient	First-order	Second-order	Third-order
γ_0	1	3/2	11/6
α_0	1	2	3
α_1	0	−1/2	−3/2
α_2	0	0	1/3
β_0	1	2	3
β_1	0	−1	−3
β_2	0	0	1

vere restriction on the size of time step, a mixed explicit–implicit method is employed where we keep the diagonal terms on the right-hand side implicit and the others explicit. In addition, we employ a high-order stiffly-stable integration scheme. To illustrate the algorithm, we denote the first term on the right-hand side of Eq. (21) as

$$\begin{aligned}&\sum_{i=0}^{M}\sum_{j=0}^{M} d_{kj}(x)\nabla\cdot[S_{ji}(x)\nabla T_i(t,x)]\\&\quad=\sum_{j=0}^{M} d_{kj}(x)\nabla\cdot[S_{jk}(x)\nabla T_k(t,x)]\\&\qquad+\sum_{j=0}^{M}\sum_{i\neq k}^{M} d_{kj}(x)\nabla\cdot[S_{ji}(x)\nabla T_i(t,x)]\\&\quad\equiv R_{1_k}(t,x)+R_{2_k}(t,x).\end{aligned}\tag{22}$$

The scheme, in matrix form, can be written as

$$\begin{aligned}&\frac{\gamma_0\mathbf{T}^{n+1}(x)-\sum_{q=0}^{J-1}\alpha_q\mathbf{T}^{n-q}(x)}{\Delta t}\\&\quad=\mathbf{R}_1^{n+1}(x)+\sum_{q=0}^{J-1}\beta_q\mathbf{R}_2^{n-q}(x)+\mathbf{D}(x)\mathbf{F}^{n+1}(x),\end{aligned}\tag{23}$$

where J is the order of accuracy in time and the superscripts $(n+1)$ and $(n-q)$ denote the time level t^{n+1} and t^{n-q}, respectively. The coefficients in the scheme are listed in Table 2 for different temporal orders. Due to the diagonal dominance of matrix $\mathbf{S}(x)$, the restriction on time step is significantly relieved. The equations in (23) are *deterministic* and can be discretized by any conventional method, e.g. finite elements, finite difference, etc. In this paper we employ the spectral/*hp* element method to obtain high accuracy in physical space [21]. Specifically, the *Jacobi polynomials*, similar to the ones used in the aforementioned chaos expansion corresponding to beta distribution, are used for spatial discretization. This produces a unified discretization in both the physical space and the random space.

5. Numerical results

In this section, we present numerical results of the generalized polynomial chaos expansion to transient heat transfer problems. We first consider a one-dimensional model problem where the exact solution is available, and subsequently we present a practical model in two dimensions of random heat conduction in electronic cooling.

5.1. One-dimensional model problem

Consider the following problem

$$\begin{aligned}&c(x;\omega)\frac{\partial T}{\partial t}=\frac{\partial}{\partial x}\left[k(x;\omega)\frac{\partial T}{\partial x}(t,x;\omega)\right]+f(t,x;\omega),\\&\quad x\in[0,1],\end{aligned}\tag{24}$$

with boundary conditions and initial condition, respectively

$$T(t,0;\omega)=T(t,1;\omega)=\cos[\epsilon(\omega)t],\quad T(0,x;\omega)=\cos(2\pi x).$$

The random heat conductivity and capacity have the forms

$$k(x;\omega)=1+\epsilon(\omega)[1+\epsilon(\omega)]x,\quad c(x;\omega)=2\pi[1+\epsilon(\omega)],\tag{25}$$

where $\epsilon(\omega)$ is a random variable, and $k(x;\omega)>0$, $c(x;\omega)>0$. The exact solution to this problem is

$$T_{\mathrm{e}}(t,x;\omega)=\cos[\epsilon(\omega)t+2\pi x],\tag{26}$$

subject to heat source $f(t,x;\omega)=4\pi^2k(x;\omega)T_{\mathrm{e}}(t,x;\omega)$. We define two error measures for the *mean* and *variance* of the numerical solution, respectively

$$\begin{aligned}&e_{\mathrm{mean}}(t,x)=|\overline{T}_{\mathrm{p}}(t,x)-\overline{T}_{\mathrm{e}}(t,x)|,\\&e_{\mathrm{var}}(t,x)=|\sigma_{\mathrm{p}}(t,x)-\sigma_{\mathrm{e}}(t,x)|,\end{aligned}$$

where $\overline{T}(t,x)=\mathbb{E}[T(t,x;\omega)]$ is the mean field and $\sigma(t,x)=\mathbb{E}[(T(t,x;\omega)-\overline{T}(t,x))^2]$ is the variance. Here $\mathbb{E}$ is the expectation operator. The subscripts 'e' and 'p' denote the exact solution and numerical solution by polynomial chaos of order p, respectively. Specifically, we examine the L_∞ norm (in physical space) of these two error measurements at time $t=1$ as the polynomial order p increases.

We assume $\epsilon(\omega)=\sigma\xi(\omega)$ in Eq. (25), where $\xi(\omega)$ is a *random variable* with standard deviation σ. Two cases are demonstrated here: $\xi(\omega)\in U(-1,1)$ is a (continuous) uniform random variable in $(-1,1)$; and $\xi(\omega)$ is a (discrete) binomial random variable with probability function $f(x;q,N)=\binom{N}{k}q^k(1-q)^{N-k}$ where $0\leqslant q\leqslant 1$, $k=0,1,\ldots,N$. The corresponding generalized polynomial chaos are, according to Table 1, *Wiener–Legendre* chaos and *Wiener–Krawtchouk* chaos, respectively. In Fig. 1 the error convergence of the two Wiener–Askey chaos is shown for different parameters. It can be seen on the semi-log scale that the numerical solutions converge exponentially fast as the expansion order p increases, for both mean and variance. The exponential

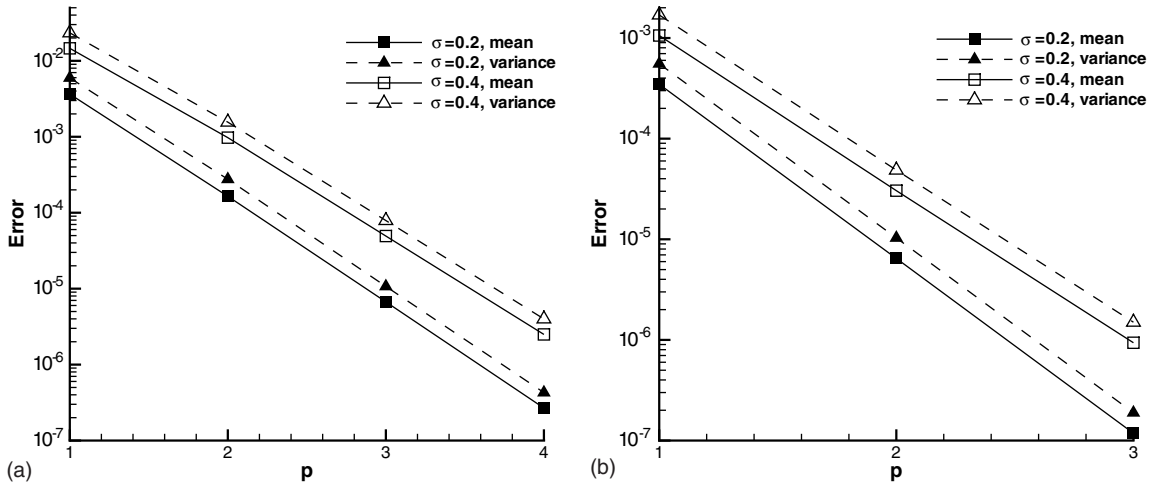

Fig. 1. Convergence of Wiener–Askey chaos for the one-dimensional model problem at $t = 1$: (a) uniform random input and Wiener–Legendre chaos and (b) binomial random input and Wiener–Krawtchouk chaos.

convergence rate is realized even for relatively large input uncertainty such as $\sigma = 0.4$, which is outside the typical effective range of perturbation methods for stochastic problems.

5.2. Random heat conduction in an electronic chip

In this section, we consider the heat conduction in an electronic chip subject to uncertainties in heat conductivity and capacity (see Eq. (13)). The computational domain D is shown in Fig. 2 along with the spatial discretization. The boundary of the domain consists of four segments: the top Γ_T, the bottom Γ_B, the two sides Γ_S and the boundaries of the cavity Γ_C, which has a depth of 0.6. Adiabatic boundary conditions are prescribed on Γ_B and Γ_S. The cavity boundary Γ_C is exposed to heat flux $q_b|_{\Gamma_C} = 1$. Two types of conditions on the top Γ_T are considered: one is maintained at constant temperature $T = 0$ (case 1) and the other is adiabatic (case 2). Due to non-zero net heat flux into the domain, there is no steady-state in case 2. The initial condition is zero everywhere. For the spectral/*hp* element solver in space, 16 elements are used in the domain, as shown in Fig. 2. Within each element, sixth-order (Jacobi) polynomials are employed. Numerical tests indicate that this is sufficient to resolve the problem in physical space. Six reference points are placed at the vertices of some chosen elements in the domain, as shown in Fig. 2. We are interested in the stochastic solution at these points and their cross-correlation coefficients. For example, the cross-correlation coefficient between reference point A and B is

$$\rho_{AB}(t) = \frac{\mathbb{E}[(T(t,x_A;\omega)-\mathbb{E}[T(t,x_A;\omega)])(T(t,x_B;\omega)-\mathbb{E}[T(t,x_B;\omega)])]}{\sigma_T(t,x_A)\sigma_T(t,x_B)}, \tag{27}$$

where $\sigma_T(t,x)$ is the standard deviation of the solution $T(t,x;\omega)$.

The uncertain heat conductivity and capacity of the medium are random fields, with mean fields $\bar{k}(x,y;\omega) =$

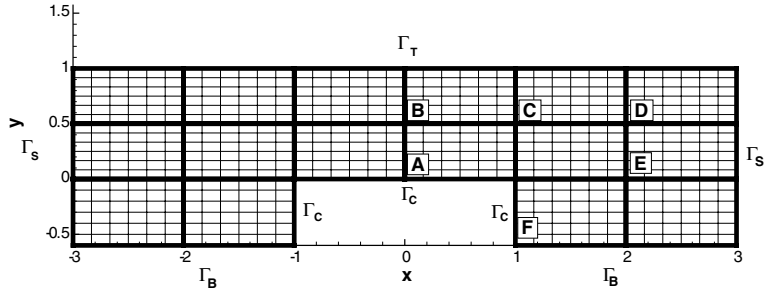

Fig. 2. Schematic of the domain of the chip geometry. It consists of 16 spectral elements of order 6 (7 points).

1, $\bar{c}(x,y;\omega)=1$ and auto-correlation functions of the form

$$C(r)=\frac{r}{b}K_1\left(\frac{r}{b}\right), \tag{28}$$

where K_1 is the modified Bessel function of the second kind with order 1, b scales as correlation length and r is the distance between two points. For any given point in the random field, this type of correlation function takes into account the influence of its nearest neighbors in *all* directions and can be considered the 'elementary' correlation in *two dimensions* [32]. Here we employ this correlation function and apply the KL decomposition of Eq. (8), following a similar procedure as in [35]. For demonstration purposes, relatively strong auto-correlations are assumed for k and c with parameter $b=20$, which results in fast decay of the eigenvalues from the KL decomposition. Subsequently, we employ the first three eigenmodes for k and the first eigenmode for c, and assume the random variables in (8) are *uniform* random variables. In Fig. 3, we plot the first two eigenmodes of the KL decomposition resulted from the numerical eigensolution of the Bessel type correlation function (28). We further assume zero cross-correlation between k and c, with uncertain intensity of $\sigma_k=\sigma_c=0.2$. This results in a *four-dimensional* ($n=4$) Wiener–Legendre chaos expansion, with three dimensions from k and one from c. Third-order ($p=3$) Legendre chaos expansion is used. Resolution checks indicate that this is sufficient to resolve the problem in random space. For $n=4$ and $p=3$, the total number of chaos expansion terms is 35 (see Eq. (18)).

We first consider case 1, where the temperature at the top boundary is maintained at $T_b|_{\Gamma_T}=0$. In this case, the temperature reaches *steady-state*. In Fig. 4 the contours of the stochastic solution of the temperature field, including the mean and standard deviation, are plotted. It is seen that the largest output uncertainty, indicated by the standard deviation, occurs near the corners between the cavity and the bottom boundary. In Fig. 5, we show the evolution of stochastic solution at the reference points, with mean on the left and COV (coefficient of variance) defined as $\mathrm{COV}(x,t)=\sigma_T(x,t)/\mathbb{E}[T(x,t;\omega)]$ on the right. We observe that the solution reaches steady-state quickly and there is a non-negligible response in COV at the early transient stage. The time evolution of cross-correlation coefficients between reference point A and the other points is shown in Fig. 6. It is seen that all the points except point B are negatively correlated with point A, and the cross correlation between A and B is weak. Note that from the definitions, the COV and cross-correlation coefficients are not defined at $t=0$, as our initial condition is zero everywhere. Thus in the following, the value of these coefficients is not plotted near $t=0$.

For the second case, we consider the *top boundary as adiabatic*. Due to the net inward heat flux from the cavity boundary, the temperature field will keep increasing and thus there is no steady-state. The equation is integrated to $t=1$ and the contours of mean field and

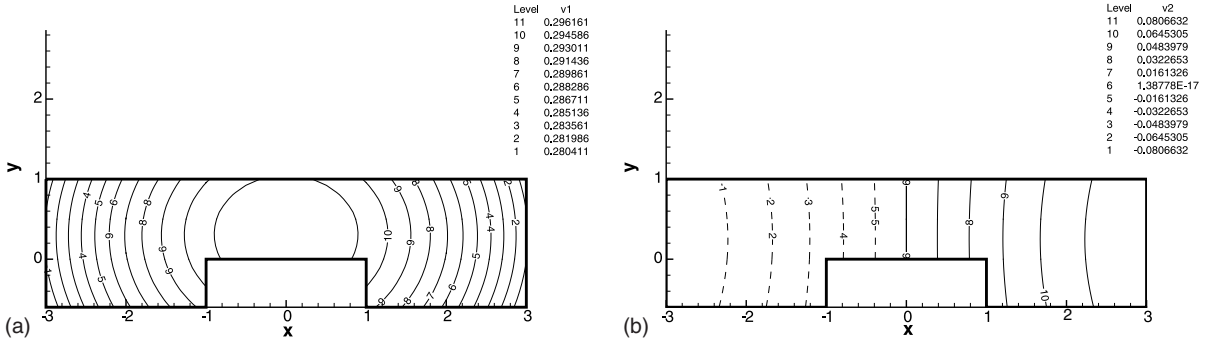

Fig. 3. Eigenmodes of the correlation field: (a) the first eigenmode and (b) the second eigenmode.

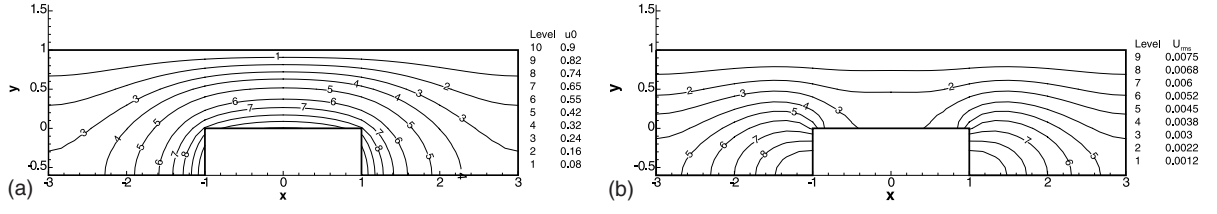

Fig. 4. Contours of temperature distribution in the electronic chip at steady-state (case 1): (a) mean field and (b) standard deviation.

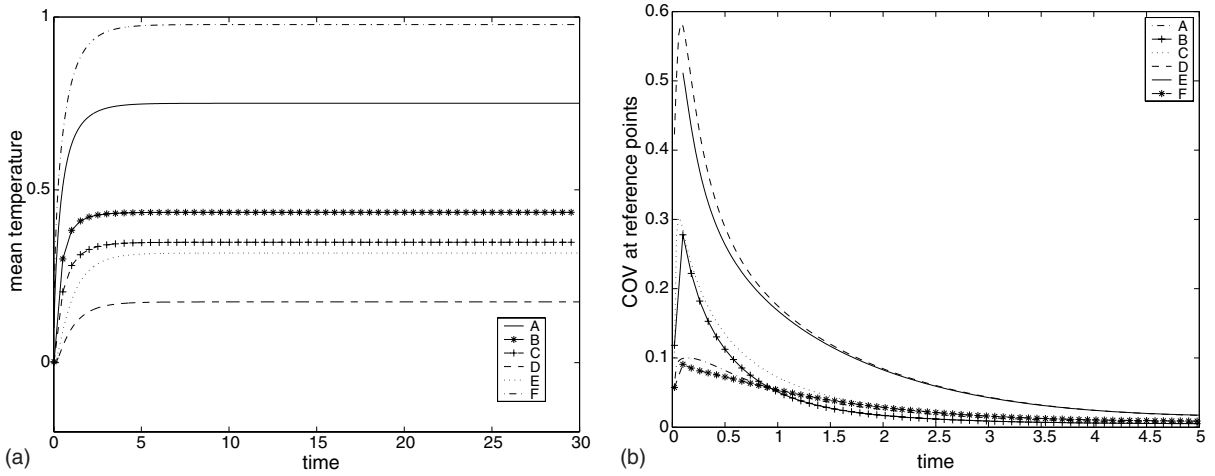

Fig. 5. Temperature evolution at reference points (case 1): (a) mean temperature and (b) COV (coefficient of variance).

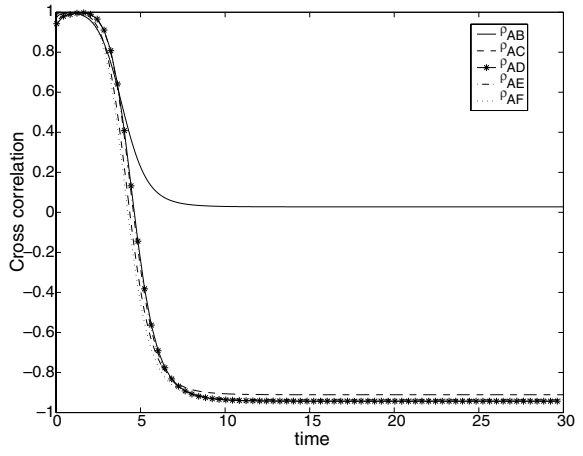

Fig. 6. Time evolution of cross-correlation coefficients between reference point A and other points (case 1).

standard deviation field are shown in Fig. 7. It is seen that the variation of the standard deviation across the width of the domain is small and the maximum value is along the vertical center line. This is qualitatively different from the steady-state solution of case 1. The solutions at reference points A–F are plotted in Fig. 8. It can be seen that while the mean temperature keeps growing over time, the COVs of temperature approach steady-state. Relatively strong variation in COV is again visible at the early transient stage. Note that the reference point F, which has the highest mean temperature, is the least sensitive to the input uncertainty. Its COV reaches steady-state very fast with value less than 10%. In Fig. 9, the cross-correlation coefficients of reference points B–F with respect to point A, are plotted. Again the statistics approach steady-state over time. In contrast to the result from case 1 in Fig. 6, all points are positively correlated to point A with strong correlation. In Fig. 10, the evolution of temperature at reference points are plotted in error bars, with the lines centered at the mean values and the length of the bars equal to two standard deviations (one up and one down).

MCS were also conducted, for both cases, to validate the results by polynomial chaos expansion. For case 1 (steady problem) we conducted 20,000 realizations. For case 2 (unsteady problem) we employed 150,000 realizations due to the shorter integration interval in time ($t = 1$). In Fig. 11, we show the evolution of solution

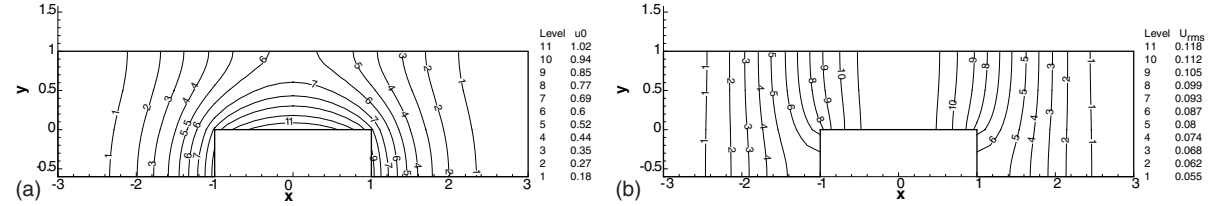

Fig. 7. Contours of temperature distribution in the electronic chip (unsteady-state at $t = 1$, case 2): (a) mean field and (b) standard deviation.

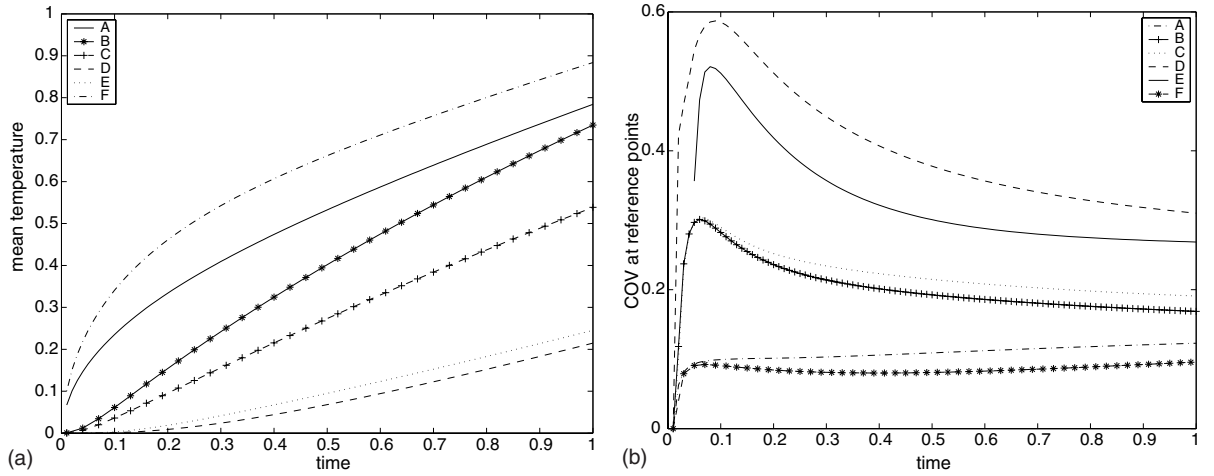

Fig. 8. Temperature evolution at reference points (case 2: unsteady problem): (a) mean temperature and (b) COV (coefficient of variance).

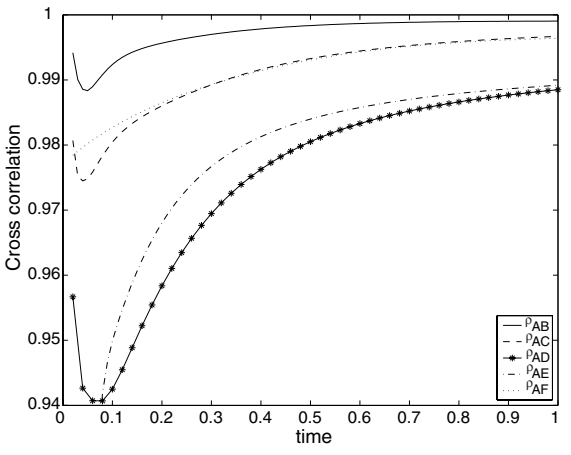

Fig. 9. Time evolution of cross-correlation coefficients between reference point A and other points (case 2: unsteady problem).

statistics at some reference points. On the left, the cross-correlation coefficients at reference points A and B for case 1 are plotted. The integration was conducted up to $t = 20$ when the solutions reach steady-state, and we show the close-up view up to $t = 6$ to focus on the early transient state. It can be seen that the results between MCS and polynomial chaos agree well; both reveal the negative cross-correlation between points A and C. The agreement between other reference points is equally good and thus it is not shown here. On the right of Fig. 11, we show, for case 2, the evolution of COVs at reference points A and D (note in this case, point D has the maximum response in COV). Again the results of MCS (150,000 realizations) agree well with those of chaos expansion. Oscillations in MCS result can be seen during the early sharp transition of point D. Good agreement is obtained for the other statistics, e.g. the mean, standard deviation and cross-correlation, and thus they are not shown here.

Another issue we are interested in is the individual effect of the uncertainty in k and c on the output for the unsteady case (case 2). Two simulations are performed with one having random conductivity k only and the other random heat capacity c only. All other parameters are the same as those in case 2. In Fig. 12 we plot the evolution of temperature COV at the reference points, with random capacity c only (left) and random conductivity k only (right). It can be seen that the COVs of the random capacity only case are smaller than those of random conductivity only, indicating the uncertainty in heat conductivity has more influence on the output than that in heat capacity, for this particular problem. Comparison on the cross-correlation coefficients are shown in Fig. 13, where we observe a stronger correlation for the random capacity only case. Note that for this unsteady problem where the temperature grows exponentially fast, the influence of heat capacity can be much more substantial if its probability distribution has unbounded support, e.g. Gaussian distribution. This was illustrated for a one-dimensional heat conduction problem in [13], and we have verified the results independently.

6. Summary

We have developed a stochastic spectral method to model uncertainty in time dependent heat conduction problems. The generalized polynomial chaos we introduced includes the original polynomial chaos, the

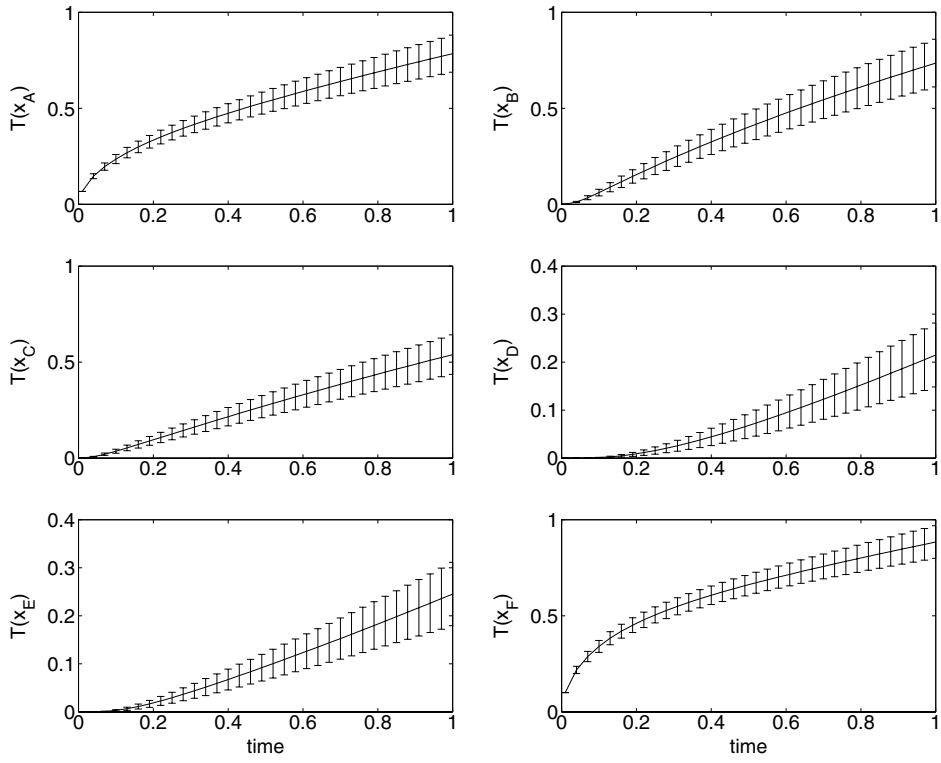

Fig. 10. Stochastic solution at reference points (case 2: unsteady problem).

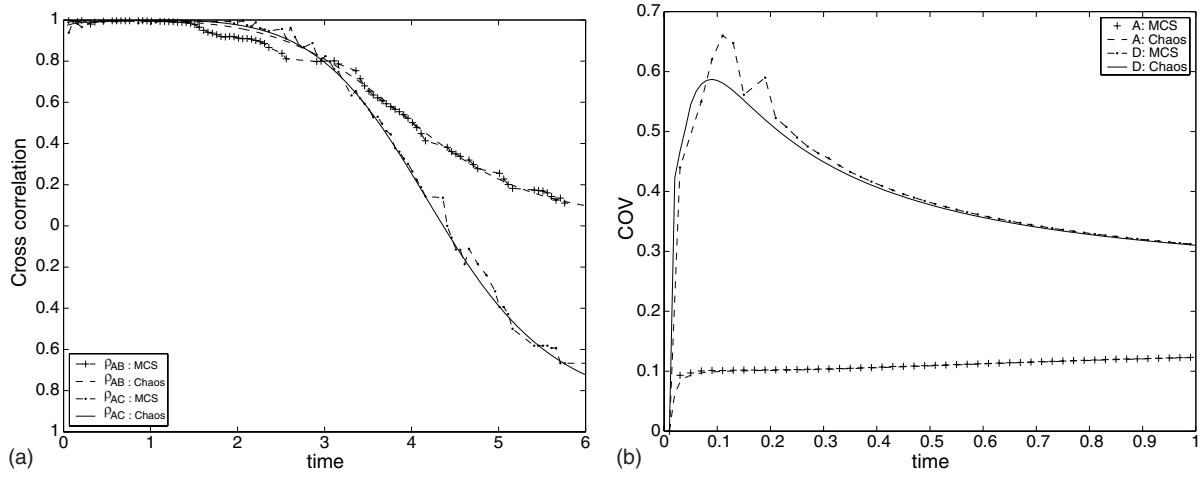

Fig. 11. Comparison of results obtained by Monte Carlo simulation and generalized polynomial chaos expansion: (a) evolution of cross-correlation coefficients at reference points for case 1 (20,00 realizations for MCS) and (b) evolution of COVs at reference points for case 2 (150,000 realizations for MCS).

Hermite chaos, as a subset, and is an extension of the original chaos idea of Wiener [33] and of the work of Ghanem and Spanos [16]. The important feature of the new broader framework is that it incorporates different types of chaos expansion corresponding to several important distribution functions, including some *discrete* distributions which cannot be readily handled by the original polynomial chaos directly.

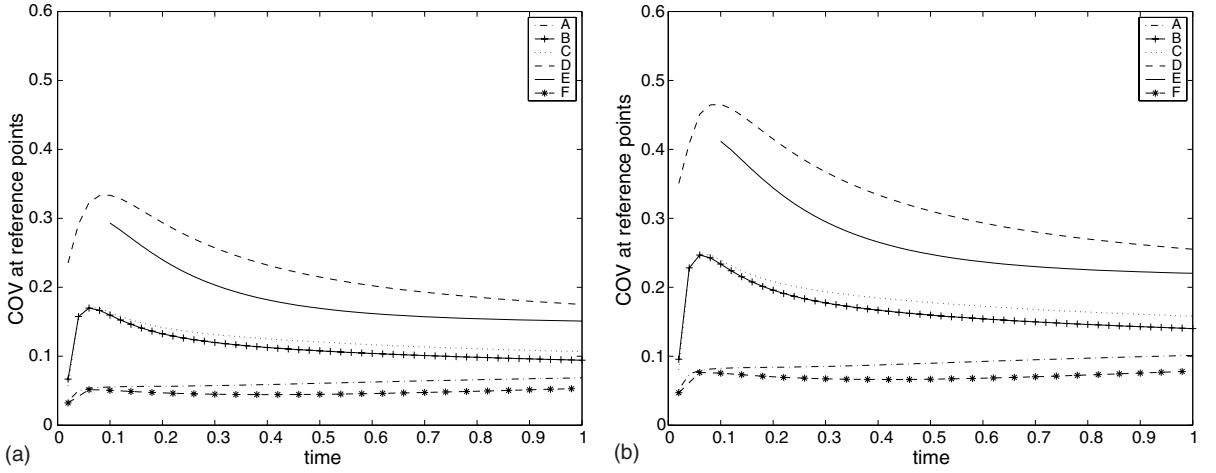

Fig. 12. Temperature COV evolution at reference points: (a) random capacity only and (b) random conductivity only.

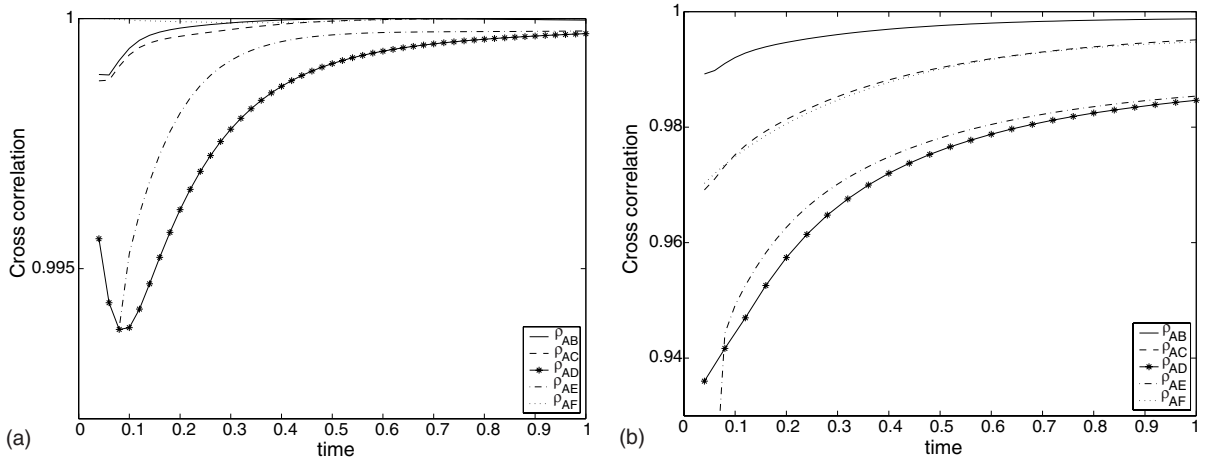

Fig. 13. Evolution of cross-correlation coefficient between reference point A and the other points: (a) random capacity only and (b) random conductivity only.

We have applied the generalized polynomial chaos to the solution of unsteady heat conduction problems, as a natural extension of our earlier work on steady-state diffusion problems [35]. We have shown that, when the appropriate chaos expansion is chosen according to the random input, the generalized polynomial chaos solution converges exponentially fast for model problem. This is in accordance with the result of [36]. Specifically, the examples presented here employ the random distributions with bounded support (uniform and binomial), so that the physical properties (heat conductivity and capacity) do not have negative values with non-zero probability. The algorithm is further applied to a more practical problem of the heat conduction of an electronic chip. Convergent results were obtained by third-order chaos expansion and various statistics are examined accordingly. MCS were conducted to validate the results by chaos expansion. At least 20,000 realizations were needed to obtain converged MCS results that agree well with those of chaos expansion. The cost of chaos expansion scales linearly with respect to the total number of expansion. For this particular problem, 35 terms were used and this resulted in more than 500 times of speed-up compared to MCS (20,000/35). For the steady-state problem (case 1), the speed-up is even more ($\sim$150,000/35) for comparable accuracy. On the other hand, the cost of the generalized polynomial chaos is about the same as that of perturbation methods. However, high-order perturbation methods are difficult to implement and they do not guarantee convergence.

The efficiency of the chaos expansion is, however, problem specific and depends greatly upon the dimensionality of the random space. Although Karhunen–Loeve decomposition, among other possible techniques, can be used to reduce the dimensionality, it can be large for systems with *very short correlation length*, e.g., the white noise. To this end, the number of expansion terms may be very large, thus reducing the efficiency of the chaos expansion drastically. This problem deserves further research.

Acknowledgements

This work was supported by DOE and NSF. Computations were performed at Brown's TCASCV and NCSA's (University of Illinois) facilities.

References

[1] R. Askey, J. Wilson, Some basic hypergeometric polynomials that generalize Jacobi polynomials, Memoris of American Mathematical Society, AMS, Providence RI, 319, 1985.
[2] I. Babuška, On randomized solutions of Laplace's equation, Casopis Pest. Mater. 36 (1961) 269–276.
[3] G.A. Bécus, F.A. Cozzarelli, The random steady-state diffusion problem. I. Random generalized solutions to Laplace's equation, SIAM J. Appl. Math. 31 (1976) 134–147.
[4] G.A. Bécus, F.A. Cozzarelli, The random steady-state diffusion problem. II: random solutions to nonlinear inhomogeneous, steady-state diffusion problems, SIAM J. Appl. Math. 31 (1976) 148–158.
[5] G.A. Bécus, F.A. Cozzarelli, The random steady-state diffusion problem. III: solutions to random diffusion problems by the method of random successive approximations, SIAM J. Appl. Math. 31 (1976) 159–178.
[6] R.H. Cameron, W.T. Martin, The orthogonal development of nonlinear functionals in series of Fourier–Hermite functionals, Ann. Math. 48 (1947) 385–392.
[7] C.R. Davis, G.M. Saidel, H. Harasaki, Sensitivity analysis of one-dimensional heat transfer in tissue with temperature-dependent perfusion, J. Biomech. Eng. 119 (1997) 77–80.
[8] M.K. Deb, I. Babuška, J.T. Oden, Solution of stochastic partial differential equations using Galerkin finite element techniques, Comput. Methods Appl. Mech. Eng. 190 (2001) 6359–6372.
[9] G. Deodatis, Weighted integral method. I: stochastic stiffness matrix, J. Eng. Mech. 117 (8) (1991) 1851–1864.
[10] G. Deodatis, M. Shinozuka, Weighted integral method. II: response variability and reliability, J. Eng. Mech. 117 (8) (1991) 1865–1877.
[11] T.D. Fadale, A.F. Emery, Transient effects of uncertainties on the sensitivities of temperatures and heat fluxes using stochastic finite elements, J. Heat Trans. 116 (1994) 808–814.
[12] R.G. Ghanem, Ingredients for a general purpose stochastic finite element formulation, Comput. Methods Appl. Mech. Eng. 168 (1999) 19–34.
[13] R.G. Ghanem, Stochastic finite elements for heterogeneous media with multiple random non-Gaussian properties, ASCE J. Eng. Mech. 125 (1) (1999) 26–40.
[14] R.G. Ghanem, R.M. Kruger, Numerical solution of spectral stochastic finite element systems, Comput. Methods Appl. Mech. Eng. 129 (1996) 289–303.
[15] R.G. Ghanem, J. Red-Horse, Propagation of uncertainty in complex physical systems using a stochastic finite elements approach, Physica D 133 (1999) 137–144.
[16] R.G. Ghanem, P. Spanos, Stochastic Finite Elements: A Spectral Approach, Springer-Verlag, New York, 1991.
[17] X. He, J.G. Georgiadis, Direct numerical solution of diffusion problems with intrinsic randomness, Int. J. Heat Mass Transfer 35 (1992) 3141–3151.
[18] T.D. Hien, M. Kleiber, Stochastic finite element modelling in linear transient heat transfer, Comput. Methods Appl. Mech. Eng. 144 (1997) 111–124.
[19] T.D. Hien, M. Kleiber, On solving nonlinear transient heat transfer problems with random parameters, Comput. Methods Appl. Mech. Eng. 151 (1998) 287–299.
[20] M. Kaminski, T.D. Hien, Stochastic finite element modeling of transient heat transfer in layered composites, Int. Commun. Heat Mass Transfer 26 (6) (1999) 801–810.
[21] G.E. Karniadakis, S.J. Sherwin, Spectral/hp Element Methods for CFD, Oxford University Press, 1999.
[22] M. Kleiber, T.D. Hien, The stochastic finite element method, John Wiley and Sons, New York, 1992.
[23] R. Koekoek, R.F. Swarttouw, The Askey-scheme of hypergeometric orthogonal polynomials and its q-analogue, Technical Report 98-17, Department of Technical Mathematics and Informatics, Delft University of Technology, 1998.
[24] J. Liu, Uncertainty analysis of temperature prediction of biological bodies subject to randomly spatial heating, J. Biomech. 34 (2001) 1637–1642.
[25] W.K. Liu, T. Belytschko, A. Mani, Probabilistic finite elements for nonlinear structural dynamics, Comput. Methods Appl. Mech. Eng. 56 (1986) 61–81.
[26] W.K. Liu, T. Belytschko, A. Mani, Random field finite elements, Int. J. Numer. Methods Eng. 23 (1986) 1831–1845.
[27] W.K. Liu, T. Belytschko, A. Mani, Applications of probabilistic finite element methods in elastic/plastic dynamics, J. Eng. Ind., ASME 109 (1987) 2–8.
[28] M. Loève, Probability Theory, fourth ed., Springer-Verlag, New York, 1977.
[29] W. Schoutens, Stochastic Processes and Orthogonal Polynomials, Springer-Verlag, New York, 2000.
[30] M. Shinozuka, G. Deodatis, Response variability of stochastic finite element systems, Technical report, Department of Civil Engineering, Columbia University, New York, 1986.
[31] E.H. Vanmarcke, M. Grigoriu, Stochastic finite element analysis of simple beams, J. Eng. Mech. 109 (1983) 1203–1214.
[32] P. Whittle, On stationary processes in the plane, Biometrika 41 (1954) 434–449.
[33] N. Wiener, The homogeneous chaos, Am. J. Math. 60 (1938) 897–936.

[34] N. Wiener, Nonlinear problems in random theory, MIT Technology Press and John Wiley and Sons, New York, 1958.
[35] D. Xiu, G.E. Karniadakis, Modeling uncertainty in steady-state diffusion problems via generalized polynomial chaos, Comput. Methods Appl. Math. Eng. 191 (2002) 4927–4948.
[36] D. Xiu, G.E. Karniadakis, The Wiener–Askey polynomial chaos for stochastic differential equations, SIAM J. Sci. Comput. 24 (2) (2002) 619–644.
[37] D. Xiu, G.E. Karniadakis, Modeling uncertainty in flow simulations via generalized polynomial chaos, J. Comput. Phys. 187 (2003) 137–167.
[38] D. Xiu, D. Lucor, C.-H. Su, G.E. Karniadakis, Stochastic modeling of flow–structure interactions using generalized polynomial chaos, J. Fluids Eng. 124 (2002) 51–59.
[39] F. Yamazaki, M. Shinozuka, G. Dasgupta, Neumann expansion for stochastic finite element analysis, Technical report, Department Civil Engineering, Columbia University, 1985.